The Cow: Discovery of a Luminous, Hot, and Rapidly Evolving Transient

Prentice, S., Maguire, K., Smartt, S., Magee, M., Schady, P., Sim, S., Chen, T-W., Clark, P., Colin, C., Fulton, M., McBrien, O., O'Neill, D., Smith, K., Ashall, C., Chambers, K. C., Denneau, L., Flewelling, H. A., Heinze, A., Holoien, T. W-S., ... Tonry, J. L. (2018). The Cow: Discovery of a Luminous, Hot, and Rapidly Evolving Transient. *The Astrophysical Journal Letters*, *865*(L3), 1-8. https://doi.org/10.3847/2041-8213/aadd90

Document Version:
Publisher's PDF, also known as Version of record

Queen's University Belfast - Research Portal:
Link to publication record in Queen's University Belfast Research Portal

CrossMark

The Cow: Discovery of a Luminous, Hot, and Rapidly Evolving Transient

S. J. Prentice[1], K. Maguire[1], S. J. Smartt[1], M. R. Magee[1], P. Schady[2], S. Sim[1], T.-W. Chen[2], P. Clark[1], C. Colin[1,3],
M. Fulton[1], O. McBrien[1], D. O'Neill[1], K. W. Smith[1], C. Ashall[4], K. C. Chambers[5], L. Denneau[5], H. A. Flewelling[5],
A. Heinze[5], T. W.-S. Holoien[6], M. E. Huber[5], C. S. Kochanek[7,8], P. A. Mazzali[9,10], J. L. Prieto[11,12], A. Rest[13,14],
B. J. Shappee[5], B. Stalder[15], K. Z. Stanek[7], M. D. Stritzinger[16], T. A. Thompson[7,8], and J. L. Tonry[5]

[1] Astrophysics Research Centre, School of Mathematics and Physics, Queen's University Belfast, BT7 1NN, UK; sipren.astro@gmail.com
[2] Max-Planck-Institut für Extraterrestrische Physik, Giessenbachstraße, D-85748, Garching, Germany
[3] Universite de Pierre et Marie Curie (Paris IV), 4 Place Jussieu, F-75252, Paris Cedex 5, France
[4] Department of Physics, Florida State University 77 Chefitan Way, Tallahasee 32304, USA
[5] Institute for Astronomy, University of Hawai'i, 2680 Woodlawn Drive, Honolulu, HI 96822, USA
[6] The Observatories of the Carnegie Institution for Science, 813 Santa Barbara Street, Pasadena, CA 91101, USA
[7] Department of Astronomy, The Ohio State University, 140 W. 18th Avenue, Columbus, OH 43210, USA
[8] Center for Cosmology and AstroParticle Physics, The Ohio State University, 191 W. Woodruff Avenue, Columbus, OH 43210, USA
[9] Astrophysics Research Institute, Liverpool John Moores University, IC2, Liverpool Science Park, 146 Brownlow Hill, Liverpool, L3 5RF, UK
[10] Max-Planck-Institut für Astrophysik, Karl-Schwarzschild-Straße 1, D-85748 Garching, Germany
[11] Núcleo de Astronomía de la Facultad de Ingeniería, Universidad Diego Portales, Av. Ejército 441, Santiago, Chile
[12] Millennium Institute of Astrophysics, Santiago, Chile
[13] Space Telescope Science Institute, 3700 San Martin Drive, Baltimore, MD 21218, USA
[14] Department of Physics and Astronomy, Johns Hopkins University, Baltimore, MD 21218, USA
[15] LSST, 950 N. Cherry Avenue, Tucson, AZ 95719, USA
[16] Department of Physics and Astronomy, Aarhus University, Ny Munkegade 120, DK-8000 Aarhus C, Denmark

Abstract

We present the ATLAS discovery and initial analysis of the first 18 days of the unusual transient event, ATLAS18qqn/AT2018cow. It is characterized by a high peak luminosity ($\sim 1.7 \times 10^{44}$ erg s^{-1}), rapidly evolving light curves (>5 mag rise to peak in ~3.5 days), and hot blackbody spectra, peaking at ~27,000 K that are relatively featureless and unchanging over the first two weeks. The bolometric light curve cannot be powered by radioactive decay under realistic assumptions. The detection of high-energy emission may suggest a central engine as the powering source. Using a magnetar model, we estimated an ejected mass of 0.1–0.4 $M_\odot$, which lies between that of low-energy core-collapse events and the kilonova, AT2017gfo. The spectra cooled rapidly from 27,000 to 15,000 K in just over two weeks but remained smooth and featureless. Broad and shallow emission lines appear after about 20 days, and we tentatively identify them as He I although they would be redshifted from their rest wavelengths. We rule out that there are any features in the spectra due to intermediate mass elements up to and including the Fe group. The presence of r-process elements cannot be ruled out. If these lines are due to He, then we suggest a low-mass star with residual He as a potential progenitor. Alternatively, models of magnetars formed in neutron star mergers, or accretion onto a central compact object, give plausible matches to the data.

Key words: stars: individual (AT2018cow) – stars: magnetars – stars: neutron – supernovae: general

1. Introduction

The advent of wide-field transient surveys that scan the visible sky every few nights has led to the discovery of new classes of transients, such as superluminous supernovae (SLSNe; e.g., Quimby et al. 2011), Type Iax SNe (e.g., Li et al. 2003), and Ca-rich transients (e.g., Perets et al. 2010). In particular, high-cadence surveys have uncovered a new parameter space of supernova-like events that rise and fall much faster than standard supernovae (SNe; e.g., Drout et al. 2014; Arcavi et al. 2016; Tanaka et al. 2016; Pursiainen et al. 2018; Rest et al. 2018). The first confirmed kilonova (AT2017gfo) from a neutron star merger detected in gravitational waves (GW170817) is the fastest declining astrophysical transient (Abbott et al. 2017) that also approaches SN-like luminosities.

These newly discovered rapidly evolving transients have a wide range of peak absolute magnitudes ($-15 > M > -22$ mag), rise times (~1–10 days), and spectral properties that make them difficult to explain through a single progenitor scenario, but most are incompatible with a radioactively powered explosion. Proposed scenarios include SN shock breakout in a surrounding wind (e.g., Ofek et al. 2010), cooling low-mass envelopes after an SN shock breakout (Nakar & Sari 2010; Kleiser & Kasen 2014), a magnetar-powered binary neutron star merger (Gao et al. 2013; Yu et al. 2013; Metzger & Piro 2014), and an optical flare from a tidal disruption event (Strubbe & Quataert 2009).

In this Letter, we report the discovery of the unusual, luminous, and fast-evolving transient, ATLAS18qqn/AT2018 cow (nicknamed "The Cow"), discovered by the ATLAS survey (Tonry et al. 2018). We present initial observations from ultra-violet (UV) to near-infrared (NIR) wavelengths out to ~18–24 days post-discovery. AT2018cow was also detected in the X-ray, radio, and submillimeter (e.g., de Ugarte Postigo et al. 2018; Rivera Sandoval et al. 2018), but these observations are not the focus of this Letter.
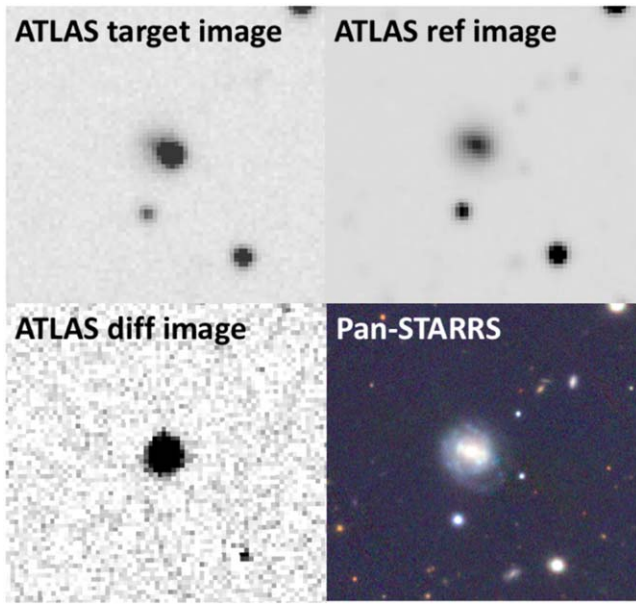
Figure 1. Images showing the location of AT2018cow: a post-discovery image (top left), a pre-discovery reference image (top right), a subtracted difference image (bottom left), and a Pan-STARRS multi-color image (bottom right).

2. Observations and Data Analysis

ATLAS is a twin 0.5 m telescope system installed on the Hawai'ian islands of Haleakala and Mauna Loa (Tonry et al. 2018). Each unit has a 28.9 square degree field of view that is robotically surveying the sky in cyan (c) and orange (o) filters that are broadly equivalent to Pan-STARRS/Sloan Digital Sky Survey (SDSS) $g+r$ and $r+i$ filters, respectively. ATLAS typically covers the whole sky visible from Hawaii every two nights. We discovered a new transient, ATLAS18qqn, in a 30 s exposure with the start time of 2018 June 16 10:35:38 UT Modified Julian Date (MJD) 58285.44141 at an AB magnitude of $o = 14.74 \pm 0.10$. It was assigned the International Astronomical Union[17] name AT2018cow and announced as an unusual transient by Smartt et al. (2018).

AT2018cow is offset by 1.7 kpc from the core of the galaxy CGCG 137-068 (Figure 1). A SDSS DR6 spectrum (Adelman-McCarthy et al. 2008; Smee et al. 2013) shows the galaxy to be star-forming with nebular emission lines at a redshift of $z = 0.014145$. A cosmology with $H_0 = 73 \text{ km s}^{-1} \text{Mpc}^{-1}$, $\Omega_m = 0.27$, and $\Omega_\Lambda = 0.73$, gives a distance of 66 ± 5 Mpc. We corrected for Milky Way (MW) extinction of $E(B-V)_{MW} = 0.08$ mag (Schlafly & Finkbeiner 2011) using a Cardelli et al. (1989) $R_V = 3.1$ extinction law. We assume that the host galaxy extinction is negligible.

ATLAS did not detect the source 3.95 days prior to the first detection to a depth of >20.2 mag (3σ limit in o band). The All Sky Automated Survey for SuperNovae (ASAS-SN; Shappee et al. 2014) did not detect the source to a depth of >18.9 mag (3σ limit in the g-band) just 1.3 days before the ATLAS detection and robustly detected the source 3 days later (see Table 1). The explosion epoch was estimated from modeling of the bolometric light curve (see Section 4) to be MJD 58284.3, with the ASAS-SN nondetection 0.2 days before.

Table 1
UVONIR Photometry of AT2018cow

MJD	Phase[a]	m	δm	Filter	Telescope
58279.50	−5.6	>20.4		c	ATLAS
58281.48	−3.9	>20.2		o	ATLAS
58284.13	−1.3	>18.9		g	ASAS-SN
58285.44	0.0	14.7	0.1	o	ATLAS
58287.15	1.6	13.40	0.05	g'	GROND
58287.15	1.6	13.8	0.1	r'	GROND
58287.15	1.6	14.1	0.1	i'	GROND
58287.15	1.6	14.32	0.05	z'	GROND
58287.15	1.6	14.71	0.07	J	GROND
58287.15	1.6	15.10	0.08	H	GROND
58287.15	1.6	15.3	0.1	K	GROND
58287.44	1.9	13.60	0.01	c	ATLAS
58288.20	2.7	13.65	0.05	g'	GROND
58288.20	2.7	14.1	0.1	r'	GROND
58288.20	2.7	14.4	0.1	i'	GROND
58288.20	2.7	14.67	0.05	z'	GROND
58288.20	2.7	15.04	0.07	J	GROND
58288.20	2.7	15.43	0.07	H	GROND
58288.20	2.7	15.6	0.1	K	GROND
58288.50	3.0	13.25	0.03	$uvw2$	UVOT
58288.50	3.0	13.32	0.04	$uvm2$	UVOT
58288.50	3.0	13.31	0.04	$uvw1$	UVOT
58288.50	3.0	13.56	0.06	Swift-u	UVOT
58288.50	3.0	13.77	0.06	Swift-b	UVOT
58288.50	3.0	13.88	0.07	Swift-v	UVOT
58288.98	3.4	13.84	0.08	u	LT
58288.98	3.4	14.12	0.06	g	LT
58288.98	3.4	14.32	0.03	r	LT
58288.98	3.4	14.76	0.03	i	LT
58289.17	3.6	14.06	0.05	g'	GROND
58289.17	3.6	14.3	0.1	r'	GROND
58289.17	3.6	14.8	0.1	i'	GROND
58289.17	3.6	15.01	0.05	z'	GROND
58289.17	3.6	15.34	0.07	J	GROND
58289.17	3.6	15.81	0.08	H	GROND
58289.17	3.6	15.9	0.1	K	GROND
58289.22	3.7	13.57	0.06	$uvw2$	UVOT
58289.22	3.7	13.60	0.07	$uvm2$	UVOT
58289.22	3.7	13.55	0.07	$uvw1$	UVOT
58289.22	3.7	13.87	0.07	Swift-u	UVOT
58289.22	3.7	14.08	0.07	Swift-b	UVOT
58289.22	3.7	14.14	0.07	Swift-v	UVOT
58289.42	3.9	14.70	0.06	o	ATLAS
58290.02	4.5	14.29	0.03	u	LT
58290.02	4.5	14.58	0.06	g	LT
58290.02	4.5	14.63	0.03	r	LT
58290.02	4.5	14.97	0.03	i	LT
58290.02	4.5	15.09	0.05	z	LT
58290.08	4.5	14.45	0.05	g'	GROND
58290.08	4.5	14.6	0.1	r'	GROND
58290.08	4.5	14.9	0.1	i'	GROND
58290.08	4.5	15.08	0.05	z'	GROND
58290.08	4.5	15.33	0.08	J	GROND
58290.08	4.5	15.57	0.08	H	GROND
58290.08	4.5	15.7	0.1	K	GROND
58290.50	4.9	14.22	0.09	$uvw2$	UVOT
58290.50	4.9	14.2	0.1	$uvm2$	UVOT
58290.50	4.9	14.16	0.07	$uvw1$	UVOT
58290.50	4.9	14.42	0.07	Swift-u	UVOT
58290.50	4.9	14.75	0.07	Swift-b	UVOT
58290.50	4.9	14.67	0.07	Swift-v	UVOT
58290.97	5.4	14.65	0.03	u	LT
58290.97	5.4	15.02	0.06	g	LT
58290.97	5.4	15.06	0.03	r	LT
58290.97	5.4	15.33	0.03	i	LT

Table 1
(Continued)

MJD	Phase[a]	m	δm	Filter	Telescope
58290.97	5.4	15.49	0.03	z	LT
58291.20	5.6	14.92	0.05	g'	GROND
58291.20	5.6	15.1	0.1	r'	GROND
58291.20	5.6	15.3	0.1	i'	GROND
58291.20	5.6	15.49	0.05	z'	GROND
58291.20	5.6	15.86	0.08	J	GROND
58291.20	5.6	16.15	0.08	H	GROND
58291.20	5.6	16.1	0.1	K	GROND
58291.43	5.9	15.34	0.03	o	ATLAS
58291.69	6.1	14.59	0.06	$uvw2$	UVOT
58291.69	6.1	14.57	0.07	$uvm2$	UVOT
58291.69	6.1	14.4	0.1	$uvw1$	UVOT
58291.69	6.1	14.70	0.07	Swift-u	UVOT
58291.69	6.1	15.02	0.08	Swift-b	UVOT
58291.69	6.1	14.96	0.08	Swift-v	UVOT
58291.98	6.4	14.85	0.07	u	LT
58291.98	6.4	15.24	0.06	g	LT
58291.98	6.4	15.32	0.03	r	LT
58291.98	6.4	15.51	0.03	i	LT
58291.98	6.4	15.62	0.03	z	LT
58292.09	6.5	14.8	0.1	$uvw2$	UVOT
58292.09	6.5	14.90	0.07	$uvm2$	UVOT
58292.09	6.5	14.76	0.08	$uvw1$	UVOT
58292.09	6.5	14.81	0.09	Swift-u	UVOT
58292.09	6.5	15.12	0.08	Swift-b	UVOT
58292.09	6.5	15.10	0.08	Swift-v	UVOT
58292.10	6.5	15.07	0.05	g'	GROND
58292.10	6.5	15.2	0.1	r'	GROND
58292.10	6.5	15.4	0.1	i'	GROND
58292.10	6.5	15.54	0.05	z'	GROND
58292.10	6.5	15.97	0.08	J	GROND
58292.10	6.5	16.30	0.09	H	GROND
58292.10	6.5	16.2	0.1	K	GROND
58292.96	7.4	15.0	0.1	u	LT
58292.96	7.4	15.43	0.06	g	LT
58292.96	7.4	15.52	0.03	r	LT
58292.96	7.4	15.66	0.03	i	LT
58292.96	7.4	15.76	0.04	z	LT
58293.12	7.5	15.28	0.05	g'	GROND
58293.12	7.5	15.5	0.1	r'	GROND
58293.12	7.5	15.6	0.1	i'	GROND
58293.12	7.5	15.74	0.05	z'	GROND
58293.12	7.5	16.12	0.08	J	GROND
58293.12	7.5	16.37	0.08	H	GROND
58293.12	7.5	16.3	0.1	K	GROND
58293.43	7.8	15.67	0.01	o	ATLAS
58293.97	8.4	15.3	0.07	u	LT
58293.97	8.4	15.65	0.06	g	LT
58293.97	8.4	15.69	0.03	r	LT
58293.97	8.4	15.82	0.03	i	LT
58293.97	8.4	15.86	0.04	z	LT
58294.13	8.5	15.45	0.05	g'	GROND
58294.13	8.5	15.6	0.1	r'	GROND
58294.13	8.5	15.7	0.1	i'	GROND
58294.13	8.5	15.77	0.05	z'	GROND
58294.13	8.5	16.0	0.1	J	GROND
58294.13	8.5	16.15	0.09	H	GROND
58294.13	8.5	16.0	0.1	K	GROND
58294.55	8.9	15.6	0.1	$uvw2$	UVOT
58294.55	8.9	15.4	0.1	$uvm2$	UVOT
58294.55	8.9	15.41	0.07	$uvw1$	UVOT
58294.55	8.9	15.44	0.08	Swift-u	UVOT
58294.55	8.9	15.59	0.08	Swift-b	UVOT
58294.55	8.9	15.57	0.09	Swift-v	UVOT

MJD	Phase[a]	m	δm	Filter	Telescope
58294.95	9.3	15.57	0.08	u	LT
58294.95	9.3	15.90	0.06	g	LT
58294.95	9.3	15.97	0.03	r	LT
58294.95	9.3	16.07	0.03	i	LT
58294.95	9.3	16.12	0.04	z	LT
58295.10	9.5	15.75	0.05	g'	GROND
58295.10	9.5	15.9	0.1	r'	GROND
58295.10	9.5	16.1	0.1	i'	GROND
58295.10	9.5	16.12	0.05	z'	GROND
58295.10	9.5	16.4	0.1	J	GROND
58295.10	9.5	16.66	0.09	H	GROND
58295.10	9.5	16.6	0.1	K	GROND
58295.55	9.9	15.8	0.1	$uvw2$	UVOT
58295.55	9.9	15.61	0.08	$uvm2$	UVOT
58295.55	9.9	15.5	0.1	$uvw1$	UVOT
58295.55	9.9	15.58	0.08	Swift-u	UVOT
58295.55	9.9	15.59	0.09	Swift-b	UVOT
58295.55	9.9	15.6	0.1	Swift-v	UVOT
58295.95	10.3	15.7	0.7	u	LT
58295.95	10.3	16.06	0.06	g	LT
58295.95	10.3	16.14	0.03	r	LT
58295.95	10.3	16.23	0.03	i	LT
58295.95	10.3	16.24	0.03	z	LT
58296.15	10.5	15.92	0.05	g'	GROND
58296.15	10.5	16.1	0.1	r'	GROND
58296.15	10.5	16.2	0.1	i'	GROND
58296.15	10.5	16.27	0.05	z'	GROND
58296.15	10.5	16.5	0.1	J	GROND
58296.15	10.5	16.70	0.09	H	GROND
58296.15	10.5	16.6	0.1	K	GROND
58296.55	10.9	16.0	0.1	$uvw2$	UVOT
58296.55	10.9	15.88	0.08	$uvm2$	UVOT
58296.55	10.9	15.75	0.08	$uvw1$	UVOT
58296.55	10.9	15.7	0.1	Swift-u	UVOT
58296.55	10.9	15.78	0.08	Swift-b	UVOT
58296.55	10.9	15.75	0.09	Swift-v	UVOT
58296.98	11.3	15.85	0.08	u	LT
58296.98	11.3	16.19	0.06	g	LT
58296.98	11.3	16.28	0.03	r	LT
58296.98	11.3	16.36	0.04	i	LT
58296.98	11.3	16.35	0.06	z	LT
58297.09	11.4	16.00	0.05	g'	GROND
58297.09	11.4	16.2	0.1	r'	GROND
58297.09	11.4	16.3	0.1	i'	GROND
58297.09	11.4	16.34	0.05	z'	GROND
58297.09	11.4	16.4	0.1	J	GROND
58297.09	11.4	16.67	0.09	H	GROND
58297.09	11.4	16.7	0.1	K	GROND
58297.43	11.8	16.5	0.2	o	ATLAS
58297.53	11.9	16.1	0.1	$uvw2$	UVOT
58297.79	12.1	16.1	0.1	$uvw2$	UVOT
58297.79	12.1	16.0	0.1	$uvm2$	UVOT
58297.79	12.1	15.8	0.1	$uvw1$	UVOT
58297.97	12.3	15.96	0.03	u	LT
58297.97	12.3	16.27	0.06	g	LT
58297.97	12.3	16.38	0.03	r	LT
58297.97	12.3	16.44	0.04	i	LT
58297.97	12.3	16.41	0.04	z	LT
58298.18	12.5	16.09	0.05	g'	GROND
58298.18	12.5	16.3	0.1	r'	GROND
58298.18	12.5	16.4	0.1	i'	GROND
58298.18	12.5	16.42	0.05	z'	GROND
58298.18	12.5	16.3	0.1	J	GROND
58298.18	12.5	16.63	0.09	H	GROND

Table 1
(Continued)

MJD	Phase[a]	m	δm	Filter	Telescope
58298.18	12.5	16.3	0.1	K	GROND
58298.20	12.5	16.2	0.1	$uvw2$	UVOT
58298.20	12.5	16.1	0.1	$uvm2$	UVOT
58298.20	12.5	15.94	0.08	$uvw1$	UVOT
58298.20	12.5	15.83	0.08	Swift-u	UVOT
58298.20	12.5	15.87	0.08	Swift-b	UVOT
58298.20	12.5	15.83	0.09	Swift-v	UVOT
58298.95	13.3	16.0	0.1	u	LT
58298.95	13.3	16.34	0.06	g	LT
58298.95	13.3	16.47	0.04	r	LT
58298.95	13.3	16.54	0.05	i	LT
58298.95	13.3	16.52	0.04	z	LT
58299.40	13.7	16.7	0.1	o	ATLAS
58299.72	14.0	16.49	0.06	$uvw2$	UVOT
58299.72	14.0	16.40	0.08	$uvm2$	UVOT
58299.72	14.0	16.1	0.1	$uvw1$	UVOT
58299.72	14.0	15.98	0.08	Swift-u	UVOT
58299.72	14.0	15.96	0.08	Swift-b	UVOT
58299.72	14.0	15.85	0.09	Swift-v	UVOT
58299.96	14.3	16.2	0.1	u	LT
58299.96	14.3	16.49	0.07	g	LT
58299.96	14.3	16.63	0.04	r	LT
58299.96	14.3	16.68	0.05	i	LT
58299.96	14.3	16.62	0.05	z	LT
58300.59	14.9	16.7	0.1	$uvw2$	UVOT
58300.59	14.9	16.63	0.09	$uvm2$	UVOT
58300.59	14.9	16.31	0.08	$uvw1$	UVOT
58300.59	14.9	16.1	0.1	Swift-u	UVOT
58300.59	14.9	16.10	0.09	Swift-b	UVOT
58300.59	14.9	16.0	0.1	Swift-v	UVOT
58300.98	15.3	16.35	0.03	u	LT
58300.98	15.3	16.62	0.06	g	LT
58300.98	15.3	16.77	0.03	r	LT
58300.98	15.3	16.83	0.03	i	LT
58300.98	15.3	16.77	0.04	z	LT
58301.64	15.9	16.9	0.1	$uvw2$	UVOT
58301.64	15.9	16.89	0.09	$uvm2$	UVOT
58301.64	15.9	16.60	0.08	$uvw1$	UVOT
58301.64	15.9	16.36	0.08	Swift-u	UVOT
58301.64	15.9	16.23	0.09	Swift-b	UVOT
58301.64	15.9	16.0	0.1	Swift-v	UVOT
58301.97	16.3	16.56	0.07	u	LT
58301.97	16.3	16.82	0.07	g	LT
58301.97	16.3	16.95	0.05	r	LT
58301.97	16.3	16.99	0.06	i	LT
58301.97	16.3	16.89	0.05	z	LT
58302.07	16.4	17.01	0.07	$uvw2$	UVOT
58302.07	16.4	16.87	0.09	$uvm2$	UVOT
58302.07	16.4	16.64	0.09	$uvw1$	UVOT
58302.07	16.4	16.35	0.09	Swift-u	UVOT
58302.07	16.4	16.19	0.09	Swift-b	UVOT
58302.07	16.4	16.2	0.1	Swift-v	UVOT

Note.
[a] Rest frame with respect to first observation.

2.1. Light Curves

We began monitoring AT2018cow starting 1.7 days after discovery (Chen & Rabus 2018; Chen & Schady 2018) in $g'r'i'z'JHK$ with GROND (Greiner et al. 2008) on the 2.2 m MPG telescope and then in $ugriz$ with IO:O on the Liverpool Telescope (LT; Steele et al. 2004) beginning 4.6 days after discovery. The optical and NIR data were calibrated using SDSS and 2MASS stars (Krühler et al. 2008). Observations with the UV Optical Telescope (UVOT; Roming et al. 2005) on board the Neil Gehrels Swift Observatory (Gehrels et al. 2004) were also obtained and were calibrated using standard procedures (Poole et al. 2008).

Figure 2 shows the multi-color light curves of AT2018cow. Maximum light occurred on MJD 58286.9 (from the light curve models, see Section 4). An ATLAS data point obtained +0.6 days from maximum has $m_c = 13.6$ mag (-20.5 mag, uncorrected for MW extinction). After peak, the light curves decayed at a rate of 0.05–0.2 mag per day, with the bluer bands typically decaying faster than the redder bands. A flattening is seen in the light curves at ~2 weeks after discovery. This flattening can be seen most clearly in the right-hand panel of Figure 2, where there is an excess in the $griz$ bolometric light curve luminosity compared to the smooth magnetar fit (see Section 4). The g-band decline between peak and 15 days post maximum is $\Delta m_{15}(g) \approx 3$ mag.

2.2. Spectroscopy

Optical spectroscopy was obtained at the LT with the low-resolution ($R \sim 350$) SPRAT spectrograph starting 2.6 days after discovery (Figure 3). The spectra were reduced using the standard LT pipeline (Barnsley et al. 2012) and a custom PYTHON script. Subsequent spectra ($R = 1000$ in the blue) were obtained at the University of Hawaii 2.2 m telescope with SNIFS (Aldering et al. 2002) and at the 4.2 m William Herschel Telescope (WHT) with ACAM (Benn et al. 2008) using a 0″.5 slit to obtain $R \sim 700$. The spectra were flux calibrated to coeval photometry.

The SNIFS spectrum shows narrow absorption features from the MW and the host galaxy, CGCG 127-68. We measured two redshifted components of the Ca II H&K lines to give a consistent redshift of $z = 0.0139$.

Analysis of the 2D spectral frames revealed that the narrow emission feature consistent with the rest wavelength of Hα is extended, leading us to conclude the emission feature in these early spectra results from the host galaxy and not AT2018cow.

The early-time spectra are blue and quite featureless, as first suggested by Perley (2018). Little evolution is seen in the spectra up to ~2 weeks after explosion, apart from a decrease in temperature. It was initially suggested that AT2018cow was spectroscopically similar to a broad-line Type Ic SN after subtraction of a power-law component (Izzo et al. 2018; Xu et al. 2018). We find that the power-law subtracted spectra of AT2018cow do not evolve similarly to the spectra of GRB-SN 1998bw (e.g., Galama et al. 1998; Patat et al. 2001). Perley et al. (2018) also present an extensive follow-up data set of AT2018cow, finding similar conclusions.

At 21.1 rest-frame days after detection (22.2 rest-frame days since explosion), the spectra of AT2018cow started to show broad features in the wavelength range of 5900–6100 Å. To aid in line identification, we calculated a series of model spectra using TARDIS, a 1D Monte Carlo radiative transfer code (Kerzendorf & Sim 2014; Kerzendorf et al. 2018). The features could be emission of He II λ4686, He I λ5015 or He II λ5005, He I λ5876, and He I λ6678, respectively (see Figure 3), but the potential emission features appear redshifted with respect to the rest position by ~3000 km s^{-1}. The identification of these features
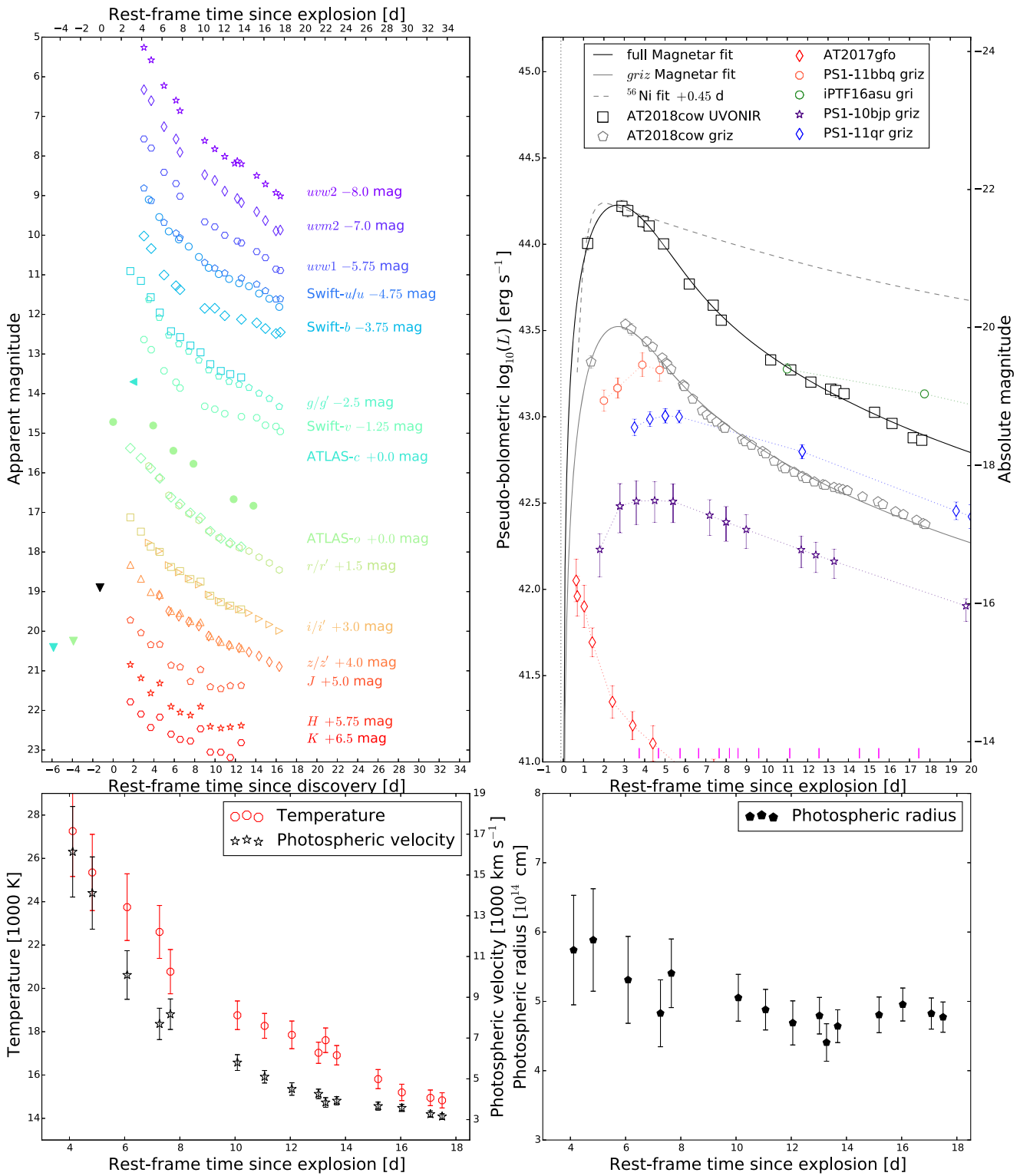
Figure 2. Upper left panel: the ATLAS, LT, GROND, and SWIFT light curves of AT2018cow. The observations are in the rest frame, with t_{exp} estimated from the light curve models. The ASAS-SN nondetection (black down arrow) is shown, along with the last ATLAS nondetections. Upper right panel: the UVONIR (black) and *griz* (gray) bolometric light curves of AT2018cow; the dotted line is the time of the ASAS-SN nondetection. Other luminous transients with short rise times are also shown: iPTF16asu (Whitesides et al. 2017), PS1-11bbq, PS1-bjp, PS1-11qr (Drout et al. 2014), and the kilonova AT2017gfo (Smartt et al. 2017). No K-corrections have been applied to the photometry. Magnetar model fits to AT2018cow are shown as a black/gray solid lines, while the best-fit ^{56}Ni-powered model is shown as a gray dashed line. Magenta lines along the bottom indicate the dates of spectral observations. Lower left panel: the effective temperature and velocity evolution of AT2018cow. Lower right panel: the photospheric radius as function of time.
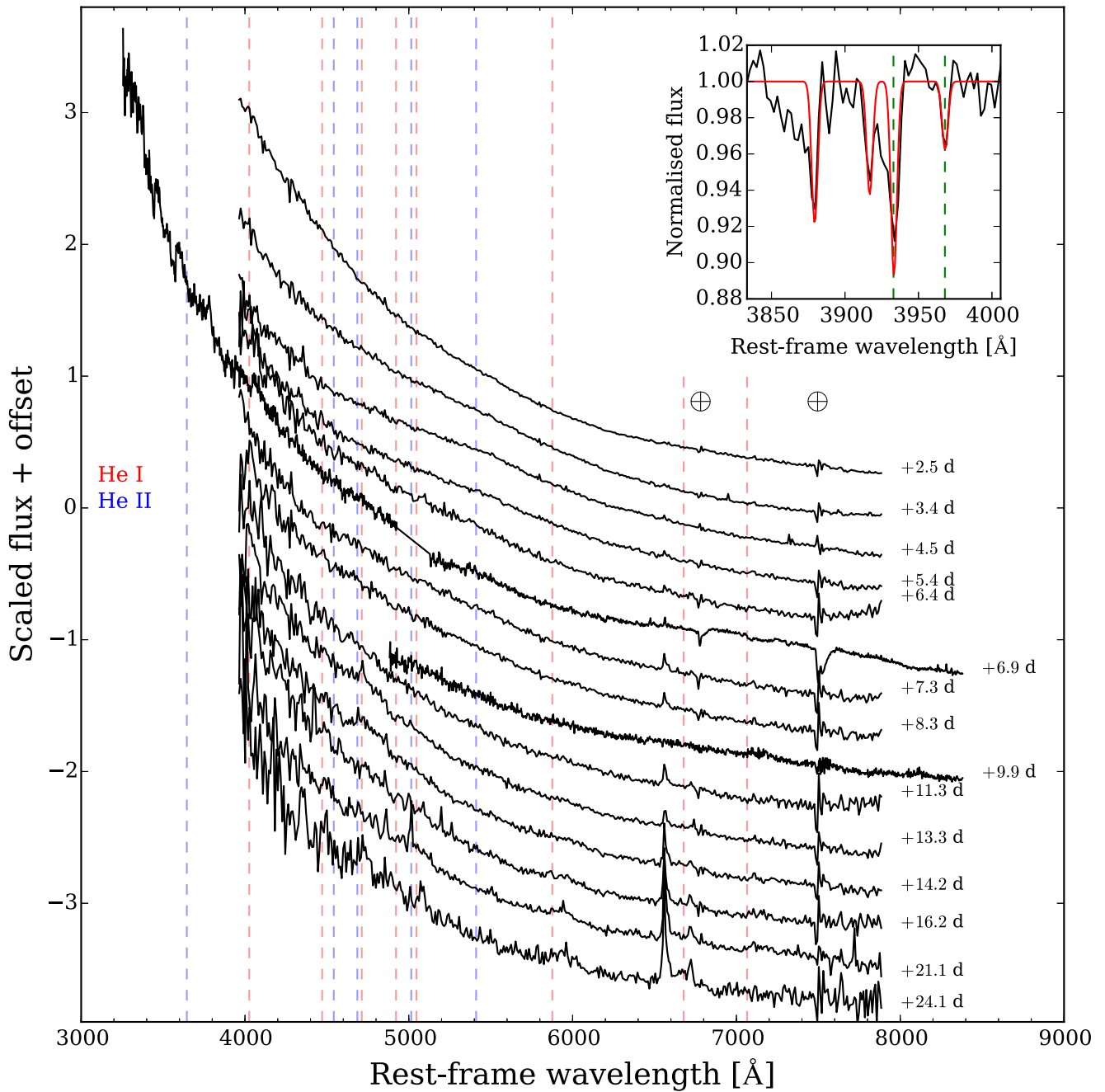
Figure 3. Spectra of AT2018cow (LT, ACAM, SNIFS) to +24.1 days, all epochs are in rest frame time since detection with the first spectrum at approximately maximum light. The inset shows the host Ca II H&K lines at $z = 0.0139$ (green dashed line).

with He I and He II, but offset to the red was also suggested by Benetti et al. (2018).

3. Temperature and Photospheric Velocity Evolution

The initial temperature of AT2018cow was estimated by modeling the spectral energy distribution as a blackbody to be $27{,}000 \pm 2000$ K at $t = 4.1$ rest-frame days since explosion (Figure 2). The temperature then shows a progressive decline over the next two weeks to $\sim$15,000 K.

Assuming homologous expansion and that AT2018cow was spherical, the photospheric velocity, v_{ph}, and photospheric radius, R_{ph}, were also estimated (Figure 2). The velocity at $t = 4.1$ days is $v_{ph} \sim 16{,}000 \pm 2000$ km s^{-1}, declining to

$\sim$3000 km s^{-1} in two weeks. Over the same period, the photospheric radius stays relatively constant at $\sim 5 \times 10^{14}$ cm.

4. Bolometric Light Curve Analysis

Figure 2 shows the pseudo-bolometric (henceforth "bolometric") light curve of AT2018cow. It was constructed using the UV to NIR photometry (UVONIR, 1850–23000 Å) and the method described in Prentice et al. (2016). Spline fits to the light curves were used to interpolate the fluxes on *SWIFT* observation dates.

AT2018cow reached a peak UVONIR luminosity, $L_p \approx 1.7 \times 10^{44}$ erg s^{-1} ($M = -21.8$ mag). Measurements of the characteristic light curve timescales using a spline fit to the data gives a rise time from $L_p/2$ to L_p of $t_{-1/2} < 1.7$ rest-frame

days and an equivalent decay time after peak of $t_{+1/2} = 2.5 \pm 0.5$ rest-frame days. Constraints from the photometric nondetections give a limit on the rise time of <3.3 days to increase >5 mag.

4.1. Model Fits to the Bolometric Light Curves

The best-fit ^{56}Ni-powered light curve model (Arnett 1982; Valenti et al. 2008) has a ^{56}Ni mass of $\sim 3\,M_\odot$ and 0.05–$0.3\,M_\odot$ of ejecta (for realistic ejecta velocities), which is unphysical. This model fits the peak luminosity and the rise, but not the decay (Figure 2), and no model fits all three.

We also investigated powering of AT2018cow by the highly magnetized, rapidly rotating neutron star (magnetar) models of Kasen & Bildsten (2010) as formulated in Inserra et al. (2013). For our model, we assumed spherical symmetry and 100% efficiency in thermalizing the spin-down energy. The best-fit model (Figure 2) has a spin period of $P \approx 11$ ms, a magnetic field strength of $B \approx 2.0 \times 10^{15}$ G, an explosion time of $t_{\rm exp} \approx 1.1$ days before the ATLAS discovery, and a rise time to maximum light of $t_{\rm rise} \approx 2.5$ days. The model fit to the *griz* light curve gives similar timescales but with $P \approx 25$ ms and $B \approx 3.5 \times 10^{15}$ G.

Using $t_{\rm rise}$, and assuming an opacity of 0.1–0.2 cm^2 g^{-1} and a kinetic energy in the range of $10^{51} < E_{\rm k} < 10^{52}$ erg, we estimated a ejecta mass of $M_{\rm ej} = 0.1$–$0.4\,M_\odot$ for the magnetar model. This lies in between the $M_{\rm ej}$ of the kilonova, AT2017gfo ($M_{\rm ej} = 0.04 \pm 0.01\,M_\odot$; Drout et al. 2017; Smartt et al. 2017), and low-mass stripped-envelope core-collapse events such as SN 1994I ($M_{\rm ej} \sim 1\,M_\odot$; Nomoto et al. 1994).

Late-time accretion onto a central compact object is predicted to roughly follow a $t^{-5/3}$ decay law (e.g., Chevalier 1989), which is similar to the t^{-2} used in the magnetar model. Therefore, a fallback accretion scenario (Dexter & Kasen 2013) for AT2018cow predicts a similar $M_{\rm ej}$.

5. Discussion and Conclusions

The combination of its high peak luminosity ($\sim 1.7 \times 10^{44}$ erg s^{-1}), fast rise time (>5 mag in 3.3 days), high peak blackbody temperature ($\sim 27{,}000$ K), low ejecta mass (0.1–$0.4\,M_\odot$), and relatively featureless and non-evolving spectra make AT2018cow very unusual. Some analogues at higher redshift may exist (Drout et al. 2014; Pursiainen et al. 2018), but discovery of events like AT2018cow are unprecedented in the local universe.

A key result of our analysis is that a magnetar or accretion model requires a low ejecta mass of ~ 0.1–$0.4\,M_\odot$, which is between that of a low-mass core-collapse event and the kilonova, AT2017gfo. From our spectral analysis, we tentatively identify emission lines of He I. The peaks of the emission features are not quite aligned with the rest frame He I wavelengths. They are redshifted, suggestive of a large bulk velocity for the He-rich material. The presence of He is difficult to reconcile with either magnetar or accretion models since such a progenitor should have previously lost all its He.

Models such as shock breakout or recombination in an extended envelope have been put forward for other fast and luminous events (e.g., Drout et al. 2014). The shock breakout of SN 1993J was nearly two magnitudes fainter than AT2018cow and required a radius of 4×10^{13} cm, already close to the limit for observed red supergiants (from calculations of Woosley et al. 1994). Therefore, an unfeasibly large and extended envelope would be required to power the light curve of AT2018cow via shock breakout. No signs of narrow line emission consistent with interaction with H/He-rich material is seen for AT2018cow, making a shock breakout from circumstellar material such as in Ofek et al. (2010) unlikely.

A number of models have been put forward for the special case of the formation of a magnetar in a binary neutron star merger (Gao et al. 2013; Yu et al. 2013; Metzger & Piro 2014). These magnetar models predict transients that are more luminous and slower evolving than kilonovae (that would occur in addition to the kilonova event). In particular, the $M_{\rm ej} = 0.1\,M_\odot$ model with a magnetic field of 10^{15} G of Metzger & Piro (2014) predicts a UV/optical transient with a similar peak luminosity, decline rate, and effective temperature to that of AT2018cow. Although published models are not a perfect match, better fits may be possible by tuning model parameters. This model also predicts nonthermal X-ray emission on a similar timescale to the UV/optical emission.

Multiple X-ray (e.g., Rivera Sandoval et al. 2018) and radio/submillimeter (e.g., de Ugarte Postigo et al. 2018) detections have been made of AT2018cow. Further modeling and observations across the full electromagnetic spectrum will hopefully allow the origin of this unusual transient to be determined.

ORCID iDs

S. J. Prentice ⓘ https://orcid.org/0000-0003-0486-6242
K. Maguire ⓘ https://orcid.org/0000-0002-9770-3508
S. J. Smartt ⓘ https://orcid.org/0000-0002-8229-1731
S. Sim ⓘ https://orcid.org/0000-0002-9774-1192
T.-W. Chen ⓘ https://orcid.org/0000-0003-1532-0149
K. C. Chambers ⓘ https://orcid.org/0000-0001-6965-7789
H. A. Flewelling ⓘ https://orcid.org/0000-0002-1050-4056
A. Heinze ⓘ https://orcid.org/0000-0003-3313-4921
M. E. Huber ⓘ https://orcid.org/0000-0003-1059-9603

C. S. Kochanek https://orcid.org/0000-0001-6017-2961
P. A. Mazzali https://orcid.org/0000-0001-6876-8284
J. L. Prieto https://orcid.org/0000-0003-0943-0026
B. J. Shappee https://orcid.org/0000-0003-4631-1149
B. Stalder https://orcid.org/0000-0003-0973-4900
M. D. Stritzinger https://orcid.org/0000-0002-5571-1833
J. L. Tonry https://orcid.org/0000-0003-2858-9657

References

Abbott, B. P., Abbott, R., Abbott, T. D., et al. 2017, ApJL, 848, L12
Adelman-McCarthy, J. K., Agüeros, M. A., Allam, S. S., et al. 2008, ApJS, 175, 297
Aldering, G., Adam, G., Antilogus, P., et al. 2002, Proc. SPIE, 4836, 61
Arcavi, I., Wolf, W. M., Howell, D. A., et al. 2016, ApJ, 819, 35
Arnett, W. D. 1982, ApJ, 253, 785
Barnsley, R. M., Smith, R. J., & Steele, I. A. 2012, AN, 333, 101
Benetti, S., Pastorello, A., Cappellaro, E., et al. 2018, ATel, 11836, 1
Benn, C., Dee, K., & Agócs, T. 2008, Proc. SPIE, 7014, 70146X
Cardelli, J. A., Clayton, G. C., & Mathis, J. S. 1989, ApJ, 345, 245
Chen, T.-W., & Rabus, M. 2018, ATel, 11729, 1
Chen, T.-W., & Schady, P. 2018, ATel, 11734, 1
Chevalier, R. A. 1989, ApJ, 346, 847
de Ugarte Postigo, A., Bremer, M., Kann, D. A., et al. 2018, ATel, 11749, 1
Dexter, J., & Kasen, D. 2013, ApJ, 772, 30
Drout, M. R., Chornock, R., Soderberg, A. M., et al. 2014, ApJ, 794, 23
Drout, M. R., Piro, A. L., Shappee, B. J., et al. 2017, Sci, 358, 1570
Galama, T. J., Vreeswijk, P. M., van Paradijs, J., et al. 1998, Natur, 395, 670
Gao, H., Ding, X., Wu, X.-F., Zhang, B., & Dai, Z.-G. 2013, ApJ, 771, 86
Gehrels, N., Chincarini, G., Giommi, P., et al. 2004, ApJ, 611, 1005
Greiner, J., Bornemann, W., Clemens, C., et al. 2008, PASP, 120, 405
Inserra, C., Smartt, S. J., Jerkstrand, A., et al. 2013, ApJ, 770, 128
Izzo, L., de Ugarte Postigo, A., Kann, D. A., et al. 2018, ATel, 11753, 1
Kasen, D., & Bildsten, L. 2010, ApJ, 717, 245
Kerzendorf, W., Nöbauer, U., Sim, S., et al. 2018, Tardis-sn/tardis: TARDIS, v2.0.2 Release, Zenodo Software Release, Zenodo, doi:10.5281/zenodo.1292315
Kerzendorf, W. E., & Sim, S. A. 2014, MNRAS, 440, 387
Kleiser, I. K. W., & Kasen, D. 2014, MNRAS, 438, 318
Krühler, T., Küpcü Yoldaş, A., Greiner, J., et al. 2008, ApJ, 685, 376
Li, W., Filippenko, A. V., Chornock, R., et al. 2003, PASP, 115, 453
Metzger, B. D., & Piro, A. L. 2014, MNRAS, 439, 3916
Nakar, E., & Sari, R. 2010, ApJ, 725, 904
Nomoto, K., Yamaoka, H., Pols, O. R., et al. 1994, Natur, 371, 227
Ofek, E. O., Rabinak, I., Neill, J. D., et al. 2010, ApJ, 724, 1396
Patat, F., Cappellaro, E., Danziger, J., et al. 2001, ApJ, 555, 900
Perets, H. B., Gal-Yam, A., Mazzali, P. A., et al. 2010, Natur, 465, 322
Perley, D. 2018, ATel, 11732, 1
Perley, D. A., Mazzali, P. A., Yan, L., et al. 2018, arXiv:1808.00969
Poole, T. S., Breeveld, A. A., Page, M. J., et al. 2008, MNRAS, 383, 627
Prentice, S. J., Mazzali, P. A., Pian, E., et al. 2016, MNRAS, 458, 2973
Pursiainen, M., Childress, M., Smith, M., et al. 2018, arXiv:1803.04869
Quimby, R. M., Kulkarni, S. R., Kasliwal, M. M., et al. 2011, Natur, 474, 487
Rest, A., Garnavich, P. M., Khatami, D., et al. 2018, NatAs, 2, 307
Rivera Sandoval, L. E., Maccarone, T. J., Corsi, A., et al. 2018, MNRAS, arXiv:1807.06369
Roming, P. W. A., Kennedy, T. E., Mason, K. O., et al. 2005, SSRv, 120, 95
Schlafly, E. F., & Finkbeiner, D. P. 2011, ApJ, 737, 103
Shappee, B. J., Prieto, J. L., Grupe, D., et al. 2014, ApJ, 788, 48
Smartt, S. J., Chen, T.-W., Jerkstrand, A., et al. 2017, Natur, 551, 75
Smartt, S. J., Clark, P., Smith, K. W., et al. 2018, ATel, 11727, 1
Smee, S. A., Gunn, J. E., Uomoto, A., et al. 2013, AJ, 146, 32
Steele, I. A., Smith, R. J., Rees, P. C., et al. 2004, Proc. SPIE, 5489, 679
Strubbe, L. E., & Quataert, E. 2009, MNRAS, 400, 2070
Tanaka, M., Tominaga, N., Morokuma, T., et al. 2016, ApJ, 819, 5
Tonry, J. L., Denneau, L., Heinze, A. N., et al. 2018, PASP, 130, 064505
Valenti, S., Benetti, S., Cappellaro, E., et al. 2008, MNRAS, 383, 1485
Whitesides, L., Lunnan, R., Kasliwal, M. M., et al. 2017, ApJ, 851, 107
Woosley, S. E., Eastman, R. G., Weaver, T. A., & Pinto, P. A. 1994, ApJ, 429, 300
Xu, D., Wang, J., Xin, L., et al. 2018, ATel, 11740, 1
Yu, Y.-W., Zhang, B., & Gao, H. 2013, ApJL, 776, L40